Journal of Power Sources 196 (2011) 8994–9007

Contents lists available at ScienceDirect

Journal of Power Sources

journal homepage: www.elsevier.com/locate/jpowsour

Novel hybrid membranes based on polybenzimidazole and ETS-10 titanosilicate type material for high temperature proton exchange membrane fuel cells: A comprehensive study on dense and porous systems

A. Eguizábal[a], J. Lemus[a], M. Urbiztondo[a], O. Garrido[b], J. Soler[a], J.A. Blazquez[b], M.P. Pina[a,*]

[a] Instituto de Nanociencia de Aragón, Universidad de Zaragoza. Campus Rio Ebro, Edificio I+D, C/Mariano Esquillor, s/n, 50018 Zaragoza, Spain
[b] CIDETEC – IK4 – Centro de Tecnologías Electroquímicas Parque Tecnológico de San Sebastián, 20009 Donostia, San Sebastián, Spain

ARTICLE INFO

Article history:
Received 1 December 2010
Received in revised form 13 February 2011
Accepted 7 March 2011
Available online 16 March 2011

Keywords:
High temperature PEM
Porous hybrid PBI based membranes
Sulfonic functionalization
Microporous fillers
Transport selectivity

ABSTRACT

Novel hybrid membranes based on polybenzimidazole (PBI) and ETS-10 titanosilicate type materials functionalized with sulfonic groups have been developed for high temperature PEMFC applications. In particular, 45% porous ETS-10/PBI electrolyte membranes in porosity have been reported for the first time in this work. A clear conduction outperforming is shown by porous PBI + 3 wt.% SO_3H-ETS-10 doped at 50 °C, attaining "in-plane" conductivity values up to 74 mS cm^{-1} at 180 °C under dry N_2 flow. The transport selectivity of the as prepared dense and porous PBI based membranes has been evaluated by comparison of "in-plane" conductivity/methanol permeability values at 50 °C, 100 °C and 150 °C. Accounting from that, dense pure PBI membranes are preferred at 50 °C (4.7×10^6 S·s·bar mol^{-1}); whereas at 150 °C, dense PBI + 3% SO_3H-ETS-10 counterparts exhibit the higher conductivity/methanol permeability ratio (2.5×10^8 S·s·bar mol^{-1}).

1. Introduction

Energy market demands reliable, low cost and low environmental impact energy sources. The development of more efficient energy conversion systems, economically feasible, is one of the most important technological challenges for the XXI century. In this context, it is expected that fuel cell systems play a key role and contribute, in a more effective way, to satisfy this urgent need. Accordingly, intensive efforts have been devoted to fuel cells area, mainly focused on costs fabrication and size/weight reduction for their use in portable and transport applications. Among FCs, proton exchange membrane fuel cells (PEMFCs) are in a favourable market situation according to the multi-annual implementation plan targets established by the Fuel Cells & Hydrogen Joint Undertaking (FCH JU) [1] to fulfill the agreements stressed by the European Strategic Agenda in Energetic Policy [2]. In this field, the research efforts are mainly focused on membrane development with good ionic conductivities at high temperatures and low humidity, low gas permeability, low electro osmotic drag coefficient, good chemical/thermal stability and mechanical properties, excellent fuel cell performance and low cost. These properties are classified into the "iron triangle" of performance, durability, and cost. Although this research topic is responsible of 90% of published works, the present development status of membranes for high temperature/low humidity operation is less than satisfactory. Current PEMFC technology is based on expensive perflourinated proton-exchange membranes that operate effectively only under fully hydrated conditions. Such expensive perfluorinated membranes could be replaced by polybenzimidazole (PBI) membranes [3,4]. This polymer has emerged as a promising candidate due to is commercially available at a relative low cost (150–220 € kg^{-1}) and exhibits excellent stability in both reductor and oxidant environments and its glass transition temperature is between 425 and 435 °C. Being a basic polymer ($pK \approx 6.0$), it easily captures acids, which help to stabilize itself. The first patent related to phosphoric acid doped PBI membranes for PEMFCs is from Savinell and Litt [5] and dates back to 1996. Since then, numerous patents emerging from this group are under exploitation. Phosphoric acid doped PBI membrane preparation is commonly made by a polymer casting process followed by a latter immersion in acid [6]. Phosphoric acid concentration and immersion time affects both physical and chemical membrane properties [7]. A high acid concentration provokes a drastic worsening in the membrane mechanical resistance [8] due to the soaking process that takes place provoking separation among the polymer chains and reduction of intermolecular interactions

* Corresponding author. Tel.: +34 976 761155; fax: +34 976 762142.
E-mail address: mapina@unizar.es (M.P. Pina).

0378-7753/$ – see front matter © 2011 Elsevier B.V. All rights reserved.
doi:10.1016/j.jpowsour.2011.03.006

[9]. Therefore, an optimal doping of the membrane implies an improvement in conductivity without affecting the mechanical properties.

Among the main strategies to improve the performance of current PBI membranes, the most studied are the following: (i) ionic cross-linking of polymeric acids and polymeric bases and later phosphoric doping to obtain a ternary system [10]; (ii) acids or halides covalently cross-linked and later phosphoric doping [11], (iii) composite organic–inorganic membranes from PBI and inorganic fillers (zirconium phosphates, phosphotungstenic acid, silicotungstenic acid, zirconium tricarboxilphosphate, polyoxometals, sulfonic silica nanoparticles) followed by phosphoric acid doping [12–16]. Recently, the characterization of highly stable, high molecular weight sulphonated PBI gel type membranes prepared using polyphosphoric acid as the reaction and casting solvent has been reported by Benicewicz et al. [17]. In comparison with sulfonated PBI or conventionally prepared PBI membranes, a pronounced increase in fuel cell performance at 160 °C is attained due to the elevated acid doping level (22–55 mol phosphoric acid/PBI) with a degradation rate of $-0.030\,mV\,h^{-1}$ in H_2/air testing.

In general, the inorganic–organic hybrid membranes are promising systems, since they have special physicochemical properties, arising from the synergic combination of both organic and hydrophilic inorganic components. In fact, higher water uptake capabilities would be expected in a composite membrane in comparison to acid–base membranes. This feature is clearly beneficial due to phosphoric acid autodehydration is a serious limitation for operation above 140 °C. In this temperature region, lower conductive oligomers like pyrophosphoric acid are generated [18]. Therefore, both conductivity and durability could be potentially enhanced in the composite membrane and, depending on the material (composition and porous structure), the reactant crossover could be even improved [19]. However, the addition of inorganic particles to a polymer results in a greater rigidity of the final polymeric membrane and eventually provokes the appearance of undesired voids at the organic–inorganic interface. Therefore, adequate surface properties coupled to low particle size are two of the main requirements for the inorganic loading to prepare electrolyte membranes with suitable transport selectivity and mechanical properties.

Functionalized microporous fillers such as Linde type A zeolite (300 nm in size) with amine groups and Beta zeolite (30–50 nm in size) with sulfonic groups have been tested in Nafion composite membranes [20] for DMFCs allowing an improvement in the conductivity/methanol permeability ratio (a 63% over pristine Nafion 117 membranes at 80 °C). To the best of our knowledge, PBI hybrid membranes containing microporous materials have been only described in the literature for gas separation applications [21]. Thus, the incorporation of nanoporous silicates in PBI dense membranes has been studied by Tsapatsis [22] to improve the H_2/CO_2 separation properties. However, the incorporation of sulphonated commercial dense silica nanoparticles (10–20 nm in diameter) to the PBI casting solution for DMFCs has been recently published [16] exhibiting conductivity/methanol permeability values of about 1.3-folds of that of the Nafion® 117 membrane used as benchmark at 25 °C. Similarly, organically modified montmorillonite clay has been successfully incorporated to a fluorine-containing PBI by Chuang et al. [23]. They reported a significant improvement of the mechanical properties and methanol permeation properties due to the addition of layered silicate to the doped PBI membrane. Nevertheless, the authors encountered that these benefits were partially offset by lower proton conductivities attributed to the diluted concentration of proton-conducting groups within the PBI nanocomposite membranes.

In this work, microporous Na/K ETS-10 crystals have been incorporated to PBI membranes for HT PEMs (up to 180 °C). Unlike microporous zeolites, where extra-framework cations are required to balance the −1 charge around tetrahedral coordinated Al; ETS-10 cations (i.e. Na, K) are principally ordered in sites adjacent to the titanate chains where they balance the two minus charge at the octahedral titanium centres. In the hydrated state, the extra-framework cations are solvated by water molecules promoting protons (H^+) transport through negative vacancies (O^{2-}) by Grotthuss mechanism [24]. Thus, higher Ti/Si atomic ratio renders in higher cation-exchange capability and higher proton conductivity values would be expected. Moreover, in comparison with LTA and MOR zeolites, ETS-10 type materials provide faster proton conduction pathways under saturated conditions [25]. Thus, ETS-10 crystals submicron in size (below 500 nm) has been synthesized following the recipe published by Rocha et al. [26]. In a step further, the external surface of ETS-10 crystals has been organically modified with sulfonic groups to: (i) promote their ionic conductivity, (ii) facilitate chemical interactions with PBI chains, (iii) improve the compatibility at the organic–inorganic interface; and, (iv) enhance the mechanical strength of the composite membranes. Finally, with the purpose of promoting even more the conductivity of hybrid membranes, porous based PBI membranes have been prepared by leaching out a low-molecular-weight compound from polymer/porogen mixtures [27,28].

In the first part of this work, preliminary experimentation on both dense and porous systems with different inorganic loadings has been carried out to define the optimal inorganic loading from "through-plane" and "in-plane" proton conductivity measurements. Pure porous and dense doped PBI membranes have also been prepared following the same procedures for comparison purposes and discussion. The second part of the work has been devoted to the study of doped membranes with the optimal SO_3H-ETS-10 inorganic loading. Particularly, "in-plane" proton conduction and methanol (vapour phase) permeability properties of hybrid porous and dense membranes have been evaluated in an attempt to identify the most adequate system for specific temperature operational windows.

2. Experimental

2.1. Synthesis and functionalization of ETS-10 crystals

In order to synthesize ETS-10 zeotype crystals with particle size around 500 nm, a gel with the following molar composition 4.4 Na_2O/1.4 K_2O/1.0 TiO_2/5.5 SiO_2/125 H_2O has been prepared. Sodium silicate (25.5–28.5% SiO_2, 7.5–8.5% Na_2O, Merck) and titanium oxide (anatase, 99.9% purity, Aldrich) have been used as Si and Ti sources, respectively, and NaCl (Merck), KCl (Panreac) and KF (Aldrich) as mineral agents. Firstly, an aqueous solution containing 0.86 g of KCl and 3.5 g of NaCl in 16.5 g of double-distilled water (DDW) is prepared. Afterwards, 12.3 g of sodium silicate are added under continuous stirring to complete dissolution. Then 1.1 g of KF is added under stirring. Finally, 0.8 g of TiO_2 (anatase) is incorporated under vigorously stirring until obtaining a homogenous and white colour gel. The homogenized gel is poured into Teflon lined autoclaves and crystallization takes place under hydrothermal conditions at 230 °C during 24 h. The material resulting is washed with DDW by centrifugation 15 min at 8500 rpm for several cycles until pH of remaining solution is less than 10. Finally, solids are ground in a mortar and stored.

External functionalization of ETS-10 crystals with sulfonic groups by grafting technique using organosilanes as coupling agents has been carried out (see Fig. 1). ETS-10 crystals are firstly dried at 200 °C during 3 h, in order to eliminate impurities and adsorbed water thus keeping free –OH groups on the surface. Afterwards, sample is introduced immediately in a three-neck round

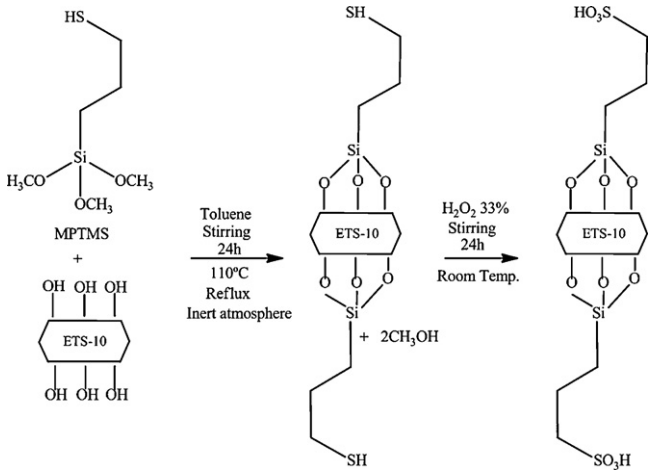

Fig. 1. Schematic representation of external sulfonation processes for ETS-10 crystals by grafting.

bottom flask and evacuated for 20 min. Finally, the three-neck round bottom flask is filled with argon to avoid the reversible hydration of the microporous material. 100 mL of dry toluene (Aldrich, 99.8 wt.%) is injected in the three-neck round bottom flask under argon atmosphere. The colloidal suspension is obtained by introducing 1 g of dried ETS-10 per 20 mL of anhydrous solvent into the three-neck round bottom flask. Afterwards, the colloidal suspension is sonicated for 15 min with all necks covered to avoid the sample hydration. Reflux equipment is firstly fixed to the second free neck of the flask bottom and the remaining free neck is used to introduce 2 mL of 3-(mercaptopropyl)trimethoxysilane (MPTMS) (Aldrich, 98.0 wt.%). Vigorous stirring and reflux under argon atmosphere are kept along the reaction time to ensure the siloxane bonds formation. The solid recovered from the organosilanation bottom flask is deeply washed with absolute ethanol (Panreac, 99.9 wt.%) for the organosilane excess removal by centrifugation. The mercapto groups grafted onto surface are further oxidized into sulfonic acid groups with 30 wt.% H_2O_2 solution (Panreac, 33 wt.%), at 25 °C for 24 h with 1:20 zeolite:H_2O_2 solution weight ratio. Extraction of excess reagents and solvent was carried out with anhydrous ethanol by centrifugation. Finally, the SO_3H-ETS-10 product is dried at 100 °C for 24 h and stored.

2.2. Preparation of PBI based membranes

Poly[2,2-(m-phenylene)-5,5-bibenzimidazole] (PBI) powder of high molecular weight purchased to FumaTech (Fumion APH) has been dissolved in an autoclave under autogenous pressure at 240 °C for 24 h. 0.5 g of PBI powder, 0.01 g of LiCl, as stabilizer, and 9.3 g of N,N-dimethylacetamide (DMAc) are mixed in the autoclave to obtain a PBI solution of 5 wt.% in DMAc. Before use, the PBI solution is filtered to remove insoluble solids from the starting PBI powder.

For the preparation of conducting polymer/ETS-10 hybrid dense membranes, the microporous material is firstly evacuated in an oven at 120 °C for at least 24 h. Afterwards, adequate amount of the organically modified inorganic solid is mixed with the PBI solution (up to 20 wt.% referred to the polymer). The resulting solution is kept under sonication for 1 h to obtain an homogeneous mixture, whereas mechanical stirring is maintained (for at least 24 h) until the casting process. The composite mixture is poured onto a glass plate of 6 or 14 cm in diameter preheated to 60 °C, in an electrical oven without convection. A heating rate of 10 °C h^{-1} is kept up to 90 °C and the membrane is maintained at this temperature for 12 h to ensure the solvent evaporation. The dried membranes are peeled off by addition of DDW. Then, LiCl stabilizer is removed by successive membrane immersion cycles into boiling water during 2 h. A series of dense films with controlled thickness between 45 and 100 μm has been obtained (see Fig. 2). The residual solvent (DMAc) is finally removed by evacuation (2 mbar) at 80 °C during 24 h. Following a similar procedure, pure dense PBI membranes have also been prepared for comparison purposes.

In the same way, porous membranes have been obtained by casting onto glass plates at room temperature from the as described PBI solution containing dibutyl phthalate (DBP) as porogen agent. Firstly, non-hybrid porous PBI membranes has been prepared as reference by adding the appropriate amount of DBP (i.e. 45 wt.% of DPB referred the polymer) to the PBI (5 wt.%) solution. Plasticized PBI films are obtained by drying on a heating plate for 1 h at room temperature, 2 h at 80 °C, 4 h at 120 °C and finally 2 h at 180 °C. Afterwards, porous polybenzimidazole films are obtained by leaching out the low-molecular-weight porogen compound using selective solvents. For such purposes, all the membranes are thoroughly washed three-fold in ethanol at 50 °C. A series of porous films with controlled thickness between 60 and 90 μm has been obtained. Using a similar procedure, hybrid porous membranes have also been prepared by addition of the inorganic loading (SO_3H-ETS-10) to the polymer solution containing the porogen agent. A schematic representation of the porous membrane preparation by this route is illustrated in Fig. 3. As it has been previously reported [27], this method allows control over the porosity level up to porosities of 75%. However, for the remaining of this work, 30% and 45% porosity membranes have been mainly studied.

Finally, the PBI based membranes have been doped with H_3PO_4 by immersion in 11 M acid solutions for more than 24 h either at low temperature (25 °C) or intermediate temperature (50 °C). Afterwards, the samples are dried with blotting paper and finally evacuated (2 mbar) at 80 °C for at least 4 h. The phosphoric acid

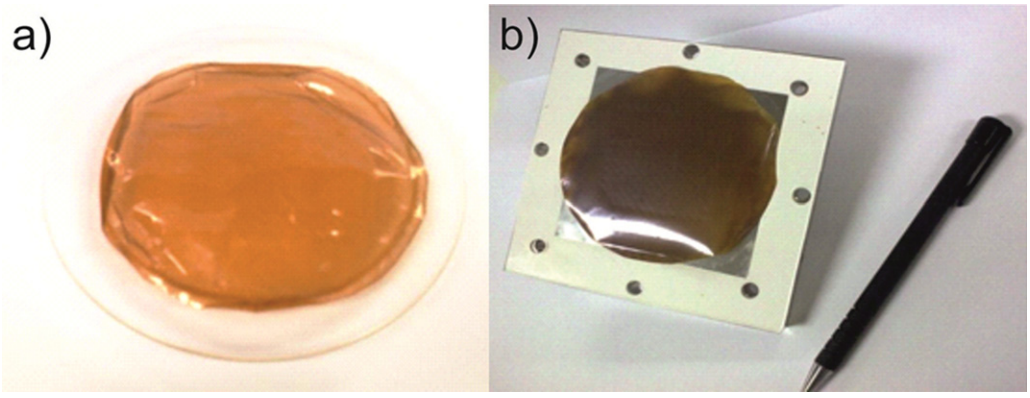

Fig. 2. External view of: (a) dense PBI membrane and (b) dense hybrid PBI membrane with 3 wt.% SO_3H-ETS-10 after phosphoric acid doping.

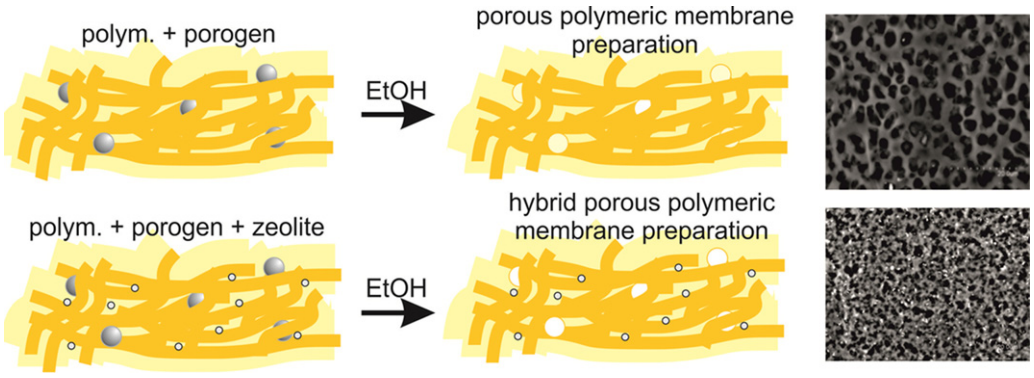

Fig. 3. Porous PBI and hybrid porous PBI films formation procedures by leaching out the porogen with ethanol.

uptake values here reported have been calculated by weight difference between doped membrane "m_{doped}" (before wiping off the phosphoric acid excess) and without doping "m_o" (after the LiCl removal), according to Eq. (1). In addition, phosphoric acid loadings have been quantified by TGA for some of the PBI based membranes prepared in this work.

$$H_3PO_4 \text{ uptake } (\%) = \frac{m_{\text{doped}} - m_0}{m_0} \times 100 \quad (1)$$

2.3. Characterization techniques

X-ray diffraction (Rigaku/Max System diffractometer Cu Kα radiation λ = 1.5418 Å, and graphite monochromator) and ATR-FTIR analyses (VERTEX 70 equipment with microscope slide MKII Golden Gate ATR from 4000 to 600 cm^{-1}, 256 scans and resolution of 0.05 cm^{-1}) were performed onto microporous ETS-10 type material to check the purity, crystallinity and organic functionalization, respectively.

Proton conductivity was determined using the complex impedance method in a closed cell. Basically, "through-plane" and "in-plane" type measurements (see Fig. 4) up to 180 °C have been carried out. In particular, "through-plane" proton conductivity of ETS-10 type materials under dry and saturated conditions has been evaluated according to the procedures already explained in our previous work [25]. On the contrary, the conduction performance of PBI based membranes has been mostly evaluated by "in-plane" measurements using a homemade four electrode conductivity station [29] under 100 mL min^{-1} of N_2. For such purposes, the doped PBI based membranes were previously conditioned for at least 2 days in a vacuum chamber at 50 °C.

Morphology, thickness, pore size and homogeneity of the as prepared membranes and functionalized microporous crystals have been studied by SEM (JEOL JSM-6400).

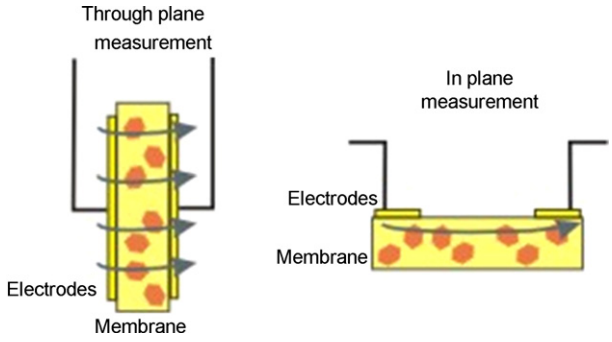

Fig. 4. Schematic representation of the "through-plane" and "in-plane" conductivity measurements.

Thermogravimetric analyses (TGA) from room temperature up to 600 °C (for ETS-10 samples) or 900 °C (for PBI based membranes) under N_2 flow and using 1 °C min^{-1} as heating rate, were performed with a Q5000 IR TGA (TA Instruments) for quantification purposes. Additionally, the surface modified ETS-10 samples were also subjected to X-Ray Photoelectron Spectroscopy (XPS). These analyses were performed with an Axis Ultra DLD (Kratos Tech.) and the spectra were excited by the monochromatized AlK_α source (1486.6 eV) run at 15 kV and 10 mA.

Methanol permeability of the as prepared membranes has been evaluated in the experimental set-up illustrated in Fig. 5 designed for membranes with 25 mm in diameter. After proper assembly and sealing of the permeation cell, the effective membrane diameter for methanol permeability is around 18 mm. The fuel cross over was examined at three different temperatures (50 °C, 100 °C and 150 °C) and atmospheric pressure. The methanol partial pressure (circa 3800 Pa) in the feed side (20 cm^3 N_2 STP min^{-1}) is controlled by means of mass-flow controllers and the thermostatic bath. On the permeate side, N_2 is also fed (20 cm^3 N_2 STP min^{-1}) as sweep gas flow. The pressure drop across the membranes is kept at 400 Pa. The methanol permeation values in vapor phase are calculated according to Eq. (2):

$$\text{permeability } (\text{mol/s} \cdot \text{m} \cdot \text{bar}) = \frac{Q_{\text{MetOH,permeate)}}}{S \cdot \Delta P_{\text{MetOH,ML}}} \times e \quad (2)$$

where $Q_{\text{MetOH,permeate}}$ is the methanol flow rate in the permeate side expressed in mol s^{-1}; S, is the effective permeation area in m^2 (i.e. 2.54×10^{-4} m^2); $\Delta P_{\text{MetOH,ML}}$ is the methanol driving pressure (mean logarithmic) across the membrane expressed in bar; e is the membrane thickness in m (around 100×10^{-6} m).

From such measurements, the experimental diffusion/solution methanol coefficients $(D/H)_{\text{MetOH}}$ have been calculated [30] at 50 °C, 100 °C and 150 °C according to Eq. (3):

$$\left(\frac{D}{H}\right)_{\text{MetOH}} (\text{mol/s} \cdot \text{m} \cdot \text{bar}) = \text{permeability } (\text{mol/s} \cdot \text{m} \cdot \text{bar}) \cdot \frac{\Delta P_{\text{MetOH,ML}} \text{ (bar)}}{P_{\text{MetOH,feed}} \text{ (bar)} - P_{\text{MetOH,permeate}} \text{ (bar)}} \quad (3)$$

where $P_{\text{MetOH,feed}}$ and $P_{\text{MetOH,permeate}}$ are the methanol partial pressure in the feed and permeate side, respectively.

3. Results and discussion

3.1. Synthesis and functionalization of ETS-10 crystals

XRD analysis of the as prepared ETS-10 type material is shown in Fig. 6 where the crystallographic ETS-10 pattern has also been inserted for comparison. In general, the experimental diffractogram fits satisfactory well the characteristic ETS-10 diffraction lines,

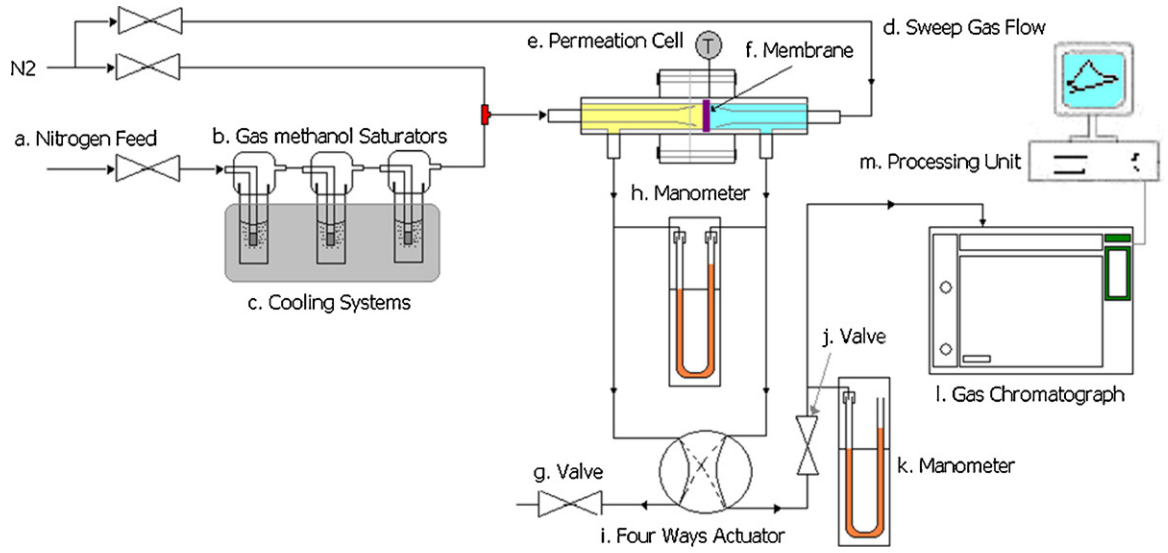

Fig. 5. Methanol permeability experimental set-up.

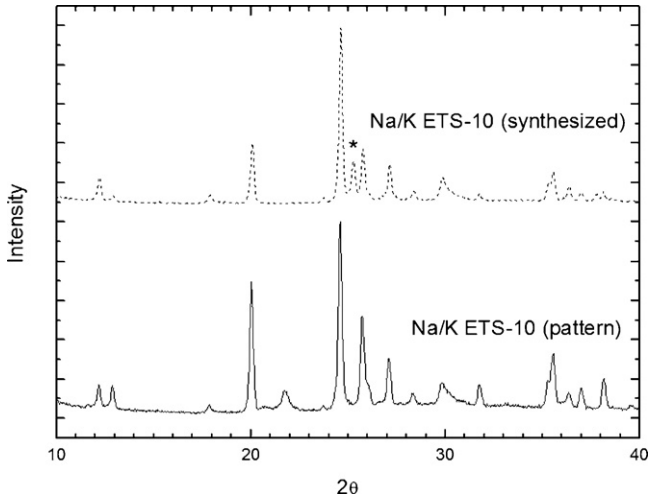

Fig. 6. XRD analysis of the synthesized Na/K ETS-10 crystals.

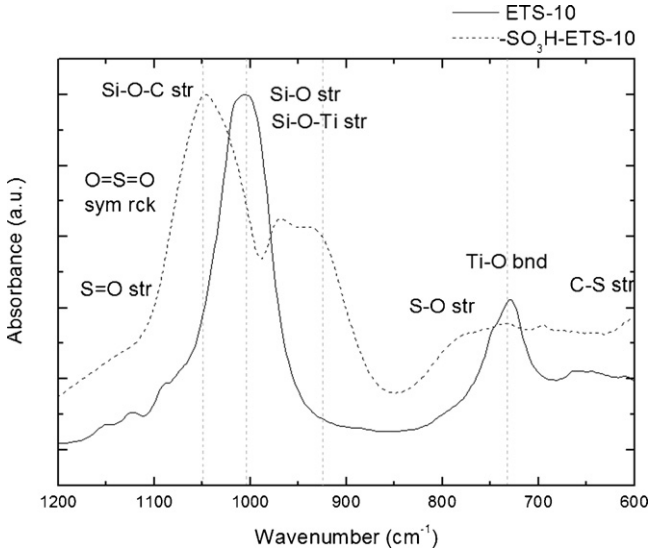

Fig. 8. ATR-FTIR analyses for Na/K ETS-10 crystals before and after sulfonation process.

although the presence of anatase impurities at $2\theta = 25.3$ (labeled in Fig. 6) could be clearly identified.

Fig. 7 shows the SEM micrographs of ETS-10 crystals revealing the typical hexagonal morphology when prepared from anatase source, and a crystal size in average below 500 nm.

The success of ETS-10 sulfonic functionalization has been evaluated by ATR-FTIR (see Fig. 8). In particular, IR characteristic bands [31] assigned to Si–O–C, O=S=O and S=O groups (1000–1200 cm^{-1}), S–O groups (700–900 cm^{-1}) and C–S groups

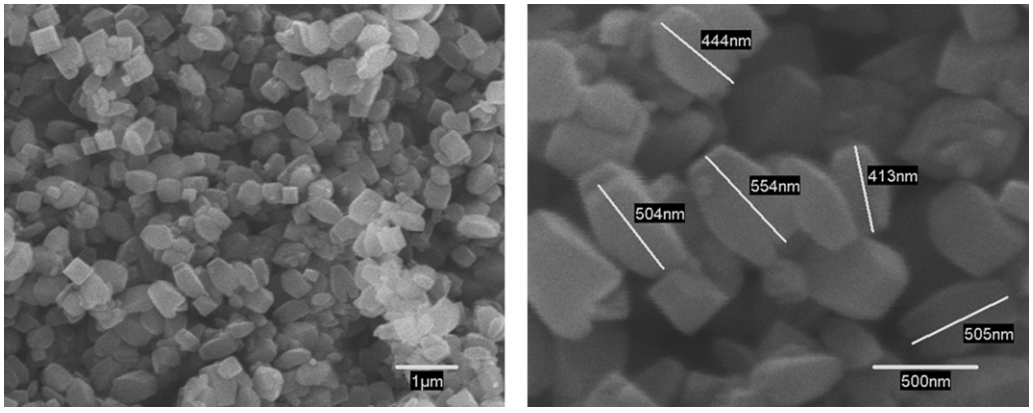

Fig. 7. SEM analysis of the synthesized Na/K ETS-10 crystals.

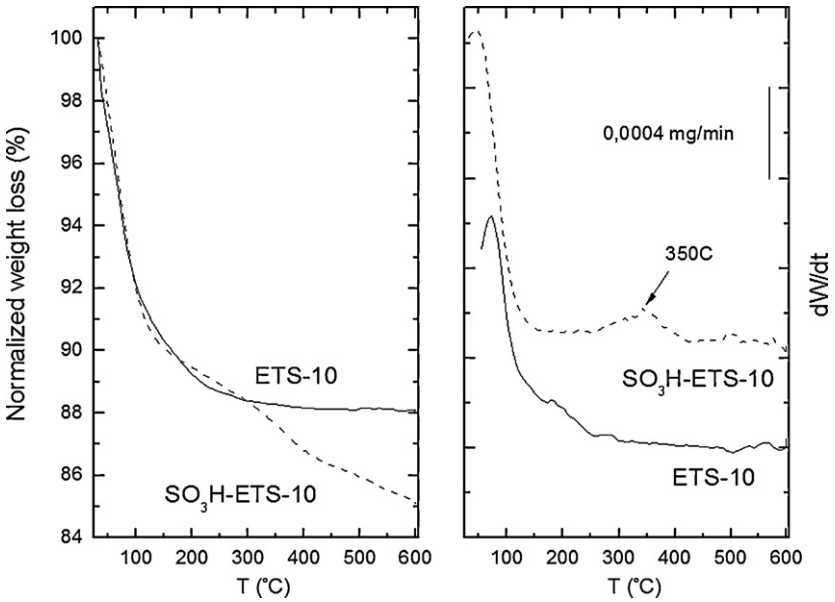

Fig. 9. TG analyses for Na/K ETS-10 crystals before and after sulfonation process.

(600–700 cm^{-1}) appear after the grafting procedure. ATR-FTIR spectra in the 1500–1600 cm^{-1} (not shown here) also reveals the presence of water.

TG analyses carried out onto Na/K ETS-10 crystals before and after sulfonation process are shown in Fig. 9 where normalized and differential curves have been depicted. The first weight loss could be associated to organics desorption and weakly bound zeolite type water. Unlike functionalized sample, this water removal is extended up to higher temperature values (300 °C) for as synthesized ETS-10 crystals. In spite of the functionalized crystals are not as efficient as bare ETS-10 for water management in order to delay phosphoric acid autodehydratation; they are providing surface groups for bonding at the interface and also additional protons and carriers for conduction. A thermal decomposition event at 350 °C associated to the organosilane removal is clearly distinguished in the differential curve for SO_3H-ETS-10 sample. Accordingly, the estimated amount of organosilane attached to the external surface of ETS10-crystals is around 4 wt.% (referred to dry solid).

Table 1 shows XPS binding energies (eV) and atomic composition (% atomic) for the most representative elements in the functionalized ETS-10 sample. By this technique, the S/Si atomic surface ratio evaluated is circa 6.4%.

The aim of organic functionalization of ETS-10 crystals is not only related to the organic-inorganic interaction at the interface; but also an improvement in the proton transport properties due to the presence of sulfonic groups is expected. Thus, experimental proton conductivity values for ETS-10 crystals before and after functionalization process at saturated conditions (100% R.H.) are presented in Fig. 10, where the behaviour exhibited at 0% R.H. has also been plotted for a better understanding.

As it is well known two possible conduction mechanisms are responsible of proton conduction in zeolites and related materials: vehicle-type and Grotthuss-type mechanisms. In the former one, the proton is transferred by a vehicle or carrier, mainly by water molecules, as hydronium cations. For the latter one, the carriers remain fixed and the proton is transferred by hopping involving an environmental rearrangement. Both mechanisms are promoted by the presence of physisorbed water. Hydrophilic zeolites exhibit a higher amount of carriers and also the extra-framework cation solvation degree is superior. This fact leads to a bigger concentration of acceptor sites (δ−) located on the anionic zeolite framework to facilite proton mobility. In addition, the presence of water molecules favors molecular interactions either hydrogen bonds or electrostatic bonds between proton acceptors (δ−) generated on the anionic backbone and the proton donors (δ+) generated as a consequence of the exchange cation solvation [24]. A similar behaviour could be reasonably expected for titanosilicate type materials. Furthermore, for SO_3H-ETS-10 crystals, the sulfonic groups grafted to the external crystal surface are able to proton transfer by the Grotthuss-type mechanism, well-known for Nafion membranes [32]. However, they could only play as proton donors in presence of a Lewis base, such as water [33,34], to ensure a continuous network [35].

As it can be observed in Fig. 10, the ionic conductivity values at dry conditions are typically of dielectric materials indicating that the contribution of hopping-type mechanism through either external surface –SO_3H groups and/or intracrystalline zeolite-type water is almost negligible in the studied temperature range.

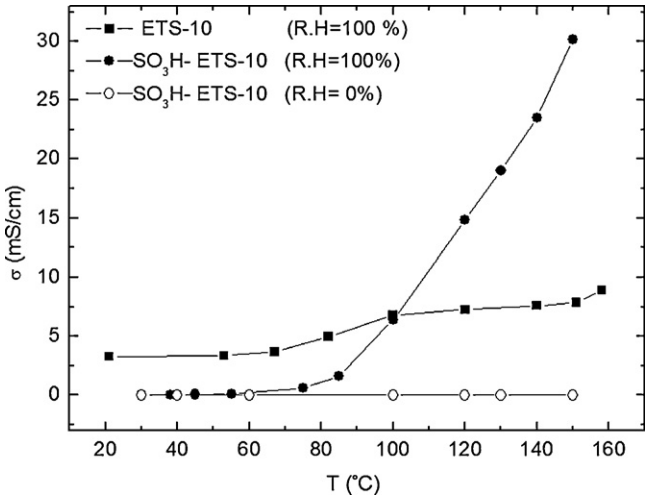

Fig. 10. Proton conductivity of Na/K ETS-10 crystals before (ETS-10) and after sulfonation process (SO_3H-ETS-10) at saturated conditions (R.H. = 100%) and dry conditions (R.H. = 0%).

Table 1
XPS analyses of the microporous ETS-10 type materials prepared.

Sample	Binding energy in eV and composition (atomic%)							Atomic ratio (%)
	O 1s	Si 2p	Ti 2p	Na 1s	K 2p	F 1s	S 2p	S/Si
HSO_3-ETS-10	532 (47.97)	102 (24.07)	459 (2.28)	1071 (4.88)	293 (1.34)	684 (0.30)	168 (1.55)	6.4

At saturated conditions, the conductivity of the as-prepared ETS-10 crystals is higher than SO_3H-ETS-10 counterparts at temperatures up to 100 °C. A possible explanation could rely on the higher water uptake values registered for bare crystals in comparison to the functionalized sample (11.9 wt.% vs. 10.8 wt.%). Nevertheless, the most distinguished feature is the proton conduction activation with temperature for SO_3H-ETS-10 samples. This fact is due to the coexistence of the two above conduction mechanisms (each of them with different activation energies) for the organic functionalized samples: vehicle-type mechanism (with H_2O as proton carrier) and hopping-type mechanism (through $-SO_3H$ terminal groups + H_2O molecules). As a result, proton conductivity values for SO_3H-ETS-10 as high as 30 mS cm^{-1} at 150 °C have been attained.

3.2. Preparation and characterization of PBI based membranes

3.2.1. Inorganic loading effect onto dense and porous PBI membranes

The experimentation carried out with hybrid ETS-10-PBI based systems processed as dense or porous membranes is herein explained. As a general rule, to assess about the benefits imposed by the inclusion of inorganic loading, pure dense or porous PBI membranes have been also prepared for comparison. According to the previous section, the surface of the microporous filler has been externally modified by means of MPTMS to: (i) improve the organic-inorganic interface because of the functional groups are prone to new type of interactions; (ii) decrease the permeability of methanol due to the enhanced polymer/inorganic interface; and, (iii) enhance the ionic conductivity of the hybrid membranes due to the interfacial voids reduction and the promotion of the ETS-10 intrinsic conductivity by the inclusion of SO_3H– terminal groups.

Firstly, a parametric study on the inorganic loading effect (from 0 wt.% to 20 wt.% referred to the polymer) onto conduction properties was carried out. Due to the acid uptake values attained at room temperature for dense systems were lower than 140% (i.e. below the commonly reported values); it was decided to alter the doping conditions to facilitate the penetration through the membrane thickness in order to achieve an homogeneous doping of PBI fibers across and along the membrane. For such purposes, the doping protocol was modified by introducing mechanical stirring and heating (50 °C) during the impregnation process with 11 M phosphoric acid solution during at least 24 h.

Fig. 11 shows the conductivity measurements from room temperature up to 180 °C using dry N_2 as sweep gas for dense PBI membranes as a function of the SO_3H-ETS-10 loading. The so obtained results correspond with "through-plane" measurements or cross conductivities. In fact, these values provide us with more realistic figures than standard "in-plane" or surface conductivity values. Therefore, if the phosphoric acid distribution is not homogeneous along the membrane thickness, the cross-section measurements would be clearly affected. Nevertheless, the exhibited "through-plane" conduction performance correlates quite well with the phosphoric acid solution uptake values: dense hybrid PBI/SO_3H-ETS-10 (3 wt.%) with 224% acid solution uptake > dense hybrid PBI/dense hybrid SO_3H-ETS-10 (20 wt.%) with 165% acid solution uptake > dense hybrid PBI/SO_3H-ETS-10 (10 wt.%) with 146% acid solution uptake > dense pure PBI with 129% acid solution uptake. Thus, the observed cross- conduction performance is in agreement with a homogenous acid distribution through the membrane thickness by doping at 50 °C under vigorous stirring.

Liu et al. [16] have reported a reduction in acid doping levels with the sulphonated silica content due to the amino groups in PBI chains are partially blocked with the sulfonic acid groups of the silica nanoparticles, decreasing the binding ability of PBI chains to H_3PO_4 molecules. In our case, the phosphoric acid solution uptake values calculated by Eq. (1) are always higher for the hybrid membranes. It is also worthwhile to remind that these figures also include the water uptake capability of the inorganic loading. (i) The relative low sulfonation degree of the ETS-10 crystals (S/Si = 0.06 atomic ratio); (ii) the intermolecular space among PBI chains generated due to the addition of ETS-10 crystals (500 nm in size); and, (iii) hydrogen bonding type interactions between phosphoric acid molecules and sulfonic terminal groups, are contributing to the exhibited behaviour in this work.

Comparing to the pristine PBI membrane, the relatively high proton conductivities of the PBI/SO_3H-ETS-10 are noteworthy (i.e. 2.2 folds for SO_3H-ETS-10 in 3 wt.% at 170 °C). This fact is due to the prevailing benefits imposed by the sulfonic acid groups grafted onto ETS-10 crystals, which contribute to a most effective acid-doping of PBI polymer and provide new proton conduction pathways. A synergic combination of both effects (i.e. lack of PBI reactivity and most effective acid-doping) occurs for PBI/SO_3H-ETS-10 with a 3 wt.% of inorganic loading, which reveals as the optimum PBI dense membrane. SEM micrographs of such membrane compared to pure dense PBI are shown in Fig. 12 to illustrate the homogeneous distribution of the inorganic particles along and across the membrane thickness.

On the other hand, the addition of the as synthesized ETS-10 in a 20 wt.% (not shown here) showed a negligible effect on the proton conductivities of the hybrid PBI dense membranes. Similar results, attributed to a dilution in the concentration of proton-conducting groups, were also reported to other nanocomposites membranes like PBI/silica membranes [36].

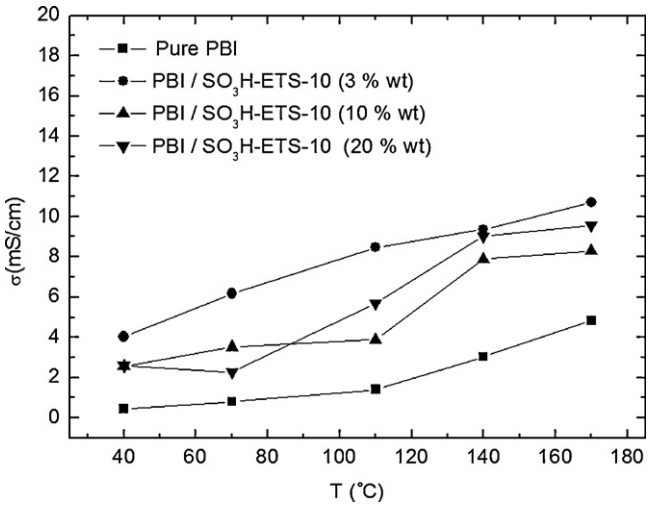

Fig. 11. "Through-plane" conductivity measurements for dense PBI membranes as a function of the SO_3H-ETS-10 loading (expressed in wt.% referred to the polymer) after phosphoric acid doping at 50 °C.

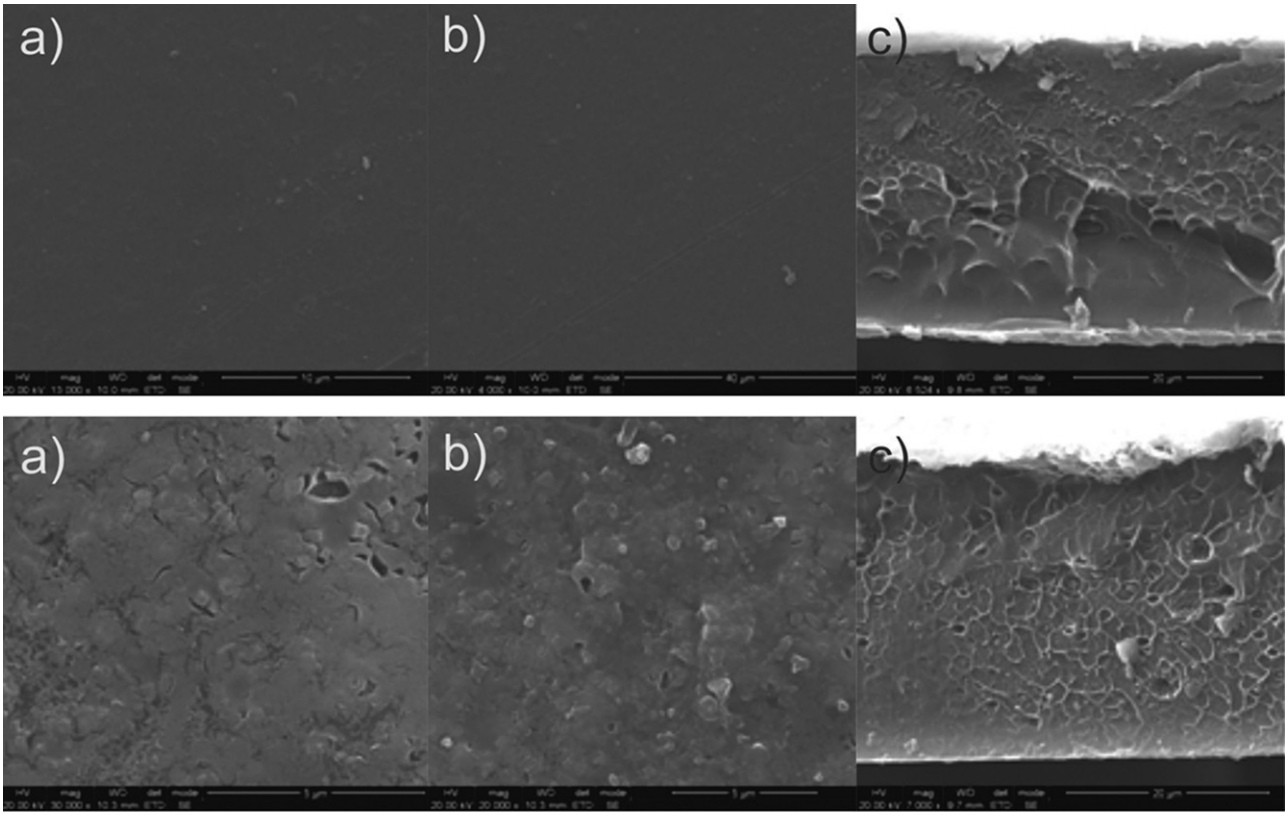

Fig. 12. SEM analyses of dense PBI systems before phosphoric acid doping: (a) bottom (glass side) surface, (b) top (air side) surface, and (c) cross section. Upper part: pure PBI membrane; lower part: hybrid PBI membrane with 3 wt.% of SO_3H-ETS-10.

The "in-plane" proton conductivities of the optimum hybrid dense membrane up to 180 °C at dry conditions are shown in Fig. 13. As it can be observed, surface conductivity values are always higher (4–5 folds) than cross conductivity values for a given temperature (i.e. 45 mS cm^{-1} vs. 11 mS cm^{-1} at 180 °C). This behaviour is explained by the presence of a phosphoric acid gel-type layer on the external surface of the membrane observed by SEM analyses (see Fig. 14) which controls the surface conduction phenomena. The bulk conductivity of pure phosphoric acid has also been evaluated in the same experimental set-up by using the specific cell for liquids. As it was expected, the proton conductivity under similar conditions is three orders of magnitude higher (i.e. 17 s cm^{-1} at 180 °C). However, for comparison purposes with available literature data, the "in-plane" conductivity performance of the as prepared membranes has been mostly studied for the remaining of this work.

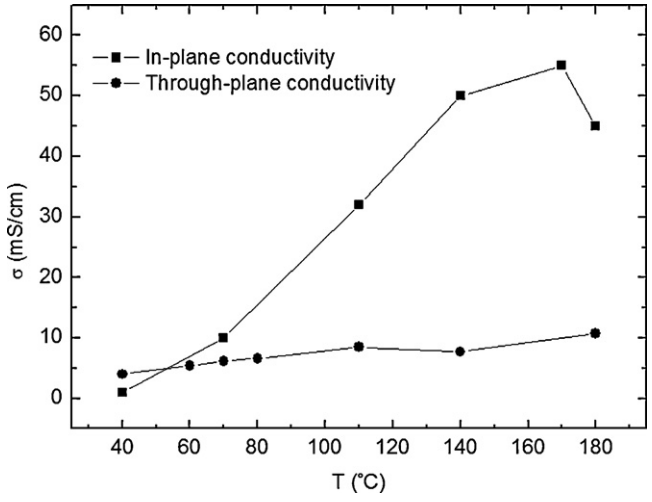

Fig. 13. "Through-plane" vs. "in-plane" conductivity measurements for dense hybrid PBI membranes with 3 wt.% of SO_3H-ETS-10 crystals.

A similar parametric study, up to 10 wt.% of inorganic loading, has been carried for porous PBI based membranes (30% in porosity) doped at 25 °C. Unlike dense series, the addition of 20 wt.% of SO_3H-ETS-10 (referred to the polymer) results in a quite heterogeneous porous membrane due to phase separation issues. Fig. 15 shows the performance of the porous set after doping at 25 °C. The conduction performance agrees with the phosphoric acid uptake values: pure porous PBI membrane with 420% acid solution uptake > porous hybrid PBI/SO_3H-ETS-10 (3 wt.%) with 185% acid solution uptake > porous hybrid PBI/SO_3H-ETS-10 (5 wt.%) with 165% acid solution uptake ~ porous hybrid PBI/SO_3H-ETS-10 (10 wt.%) with 165% acid solution uptake. The most remarkable feature is the elevated phosphoric acid uptake value exhibited by the 30% porous membrane. This behaviour could be explained by the scarce degree of pore-connectivity typical of this porosity level [27], and consequently, by the low probability of proton conductor leakage during handling.

Unlike dense systems, a negative effect of the inorganic loading onto the phosphoric acid uptake values is observed. Thus, the hybrid porous membranes (30% in porosity) retain quite less amount of phosphoric acid than the porous PBI counterpart (185% vs. 420%). A possible explanation could rely on the fact that the external surface area of porous membranes for phosphoric acid doping is higher than dense counterparts. Accordingly the "negative" contribution of sulfonic-amino interactions between the inorganic filler and the imidazol rings from PBI chains on the doping stage prevails over the "positive" sulfonic-phosphoric acid interactions. Furthermore, in spite of the doping levels discrepancies,

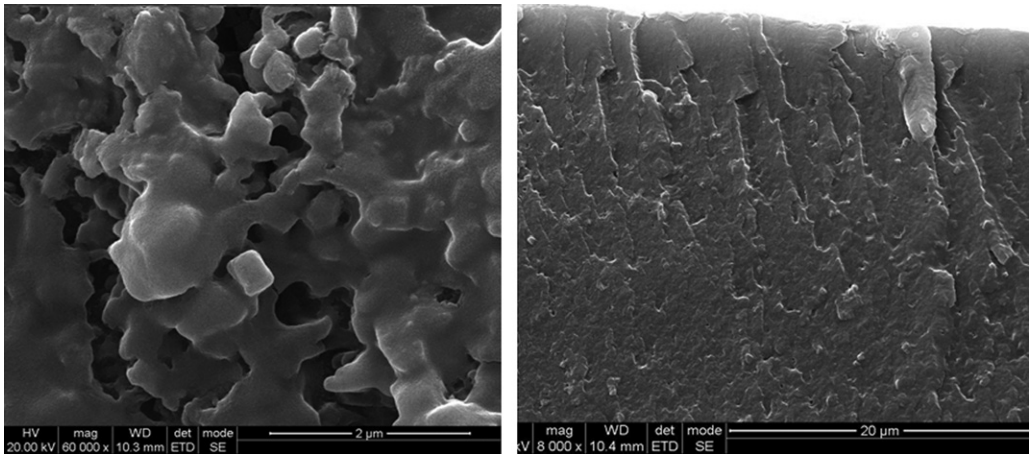

Fig. 14. SEM analyses of dense hybrid PBI membrane with 3 wt.% of SO_3H-ETS-10 crystals after phosphoric acid doping: (left) top surface and (right) cross section.

all the porous membranes exhibit a rather similar conductivity-temperature pattern: pure porous PBI membrane – 53 mS cm^{-1} at 160 °C ∼ hybrid porous PBI/SO_3H-ETS-10 (3 wt.%) – 50 mS cm^{-1} at 160 °C > hybrid porous PBI/SO_3H-ETS-10 (5 wt.%) – 44 mS cm^{-1} at 160 °C > hybrid porous PBI/SO_3H-ETS-10 (10 wt.%) – 40 mS cm^{-1} at 160 °C. This observation is also supporting the scarce degree of connectivity between pores filled with phosphoric acid, already pointed out. Therefore, and alike dense systems, the porous hybrid PBI membrane with a 3% of SO_3H-ETS-10 emerges as the most adequate among the tested due to the conduction performance is almost similar to pure porous PBI but at a clearly lower H_3PO_4 doping levels (185% vs. 420%). Consequently, improved durability properties will be expected for the composite sample. In the next section, 45% porous PBI based membranes are discussed to assess about the advantages of higher porosity levels.

3.2.2. *Proton conductivity and methanol permeability for hybrid PBI based systems: dense vs. porous membranes*

Accounting from previous section, the results concerning with hybrid SO_3H-ETS-10-PBI based systems (3 wt.% inorganic loading) processed as dense or porous (45% in porosity) membranes are herein explained and compared with pure PBI counterparts. Table 2 compiles the acid doping levels of the fully studied membranes in this section. All the samples were introduced for at least 2 days in a vacuum chamber at 50 °C for stabilization purposes before IES analysis at different temperatures and under 100 ml min^{-1} of N_2. As it was expected, for a given data set, those membranes doped at 50 °C exhibit enhanced conduction performance (see Figs. 16 and 17) in accordance with their slightly higher phosphoric acid uptake values tabulated.

The "in-plane" conduction performance for dense PBI based membranes is depicted in Fig. 16. In spite of the higher concentration of proton conductors attained for both hybrid PBI/SO_3H-ETS-10 membranes, the conductivity values are always below the pure dense PBI counterparts. This observation could be explained by the type of conductivity measurements carried out. As a matter of fact, the "in-plane" conduction performance is fully controlled by the acid gel-type layer formed onto both membrane sides (already shown in Fig. 14). Therefore, as the concentration of proton conductors onto the external surface of the hybrid membranes is lower due to SO_3H-ETS-10 crystals are partially blocking the PBI reactivity, the conductivity values are being hampered. Consequently, pure PBI membrane doped at 50 °C emerges as the most adequate among the tested dense membranes (72 mS cm^{-1} at 170 °C).

Similarly, Fig. 17 shows the "in-plane" conduction performance for porous PBI based membranes. Firstly, it is worthwhile to notice the lower phosphoric acid uptake values registered for 45% porous

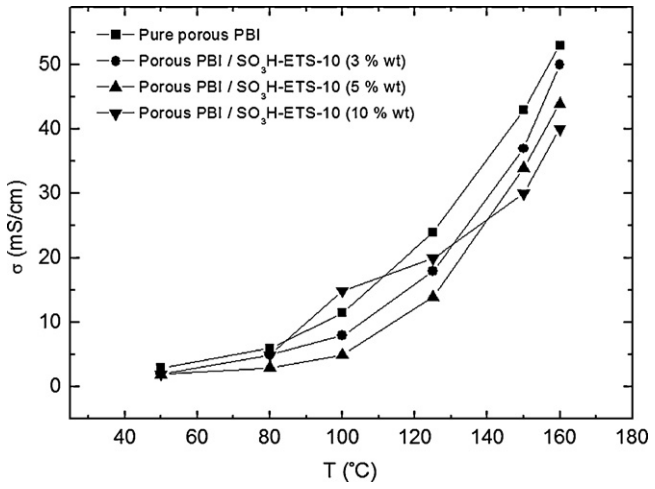

Fig. 15. "In-plane" conductivity measurements for porous PBI membranes (30% in porosity) as a function of the SO_3H-ETS-10 loading (expressed in wt.% referred to the polymer) after phosphoric acid doping at 25 °C.

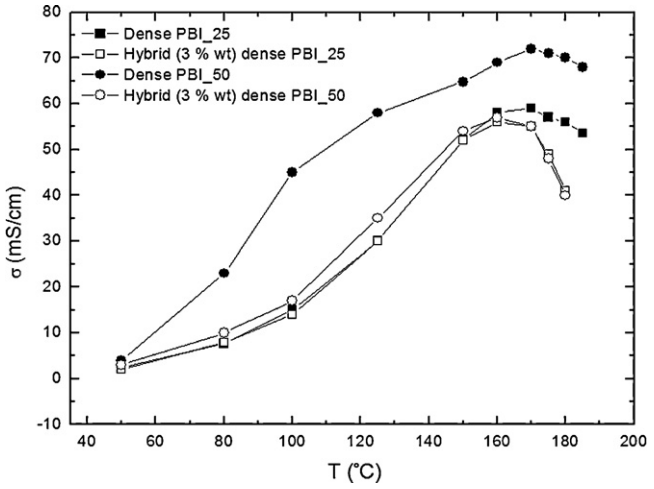

Fig. 16. "In-plane" conductivity measurements of dense systems after phosphoric acid doping at 25 °C and 50 °C: pure PBI membrane vs. hybrid PBI membrane with 3 wt.% of SO_3H-ETS-10.

Table 2
Main characteristics for some of the PBI based membranes prepared.

Nomenclature	Inorganic loading (%)[a]	DBP content (%)[b]	Acid doping temperature (°C)	H_3PO_4 uptake (%)[c]
Dense PBI_25	0%	0%	25 °C	126
Dense PBI_50	0%	0%	50 °C	129
Hybrid (3 wt.%) dense PBI_25	3%	0%	25 °C	153
Hybrid (3 wt.%) dense PBI_50	3%	0%	50 °C	157
Porous (45 wt.%) PBI_25	0%	45%	25 °C	202
Porous (45 wt.%) PBI_50	0%	45%	50 °C	220
Hybrid (3 wt.%) porous (45% DBP) PBI_25	3%	45%	25 °C	264
Hybrid (3 wt.%) porous (45% DBP) PBI_50	3%	45%	50 °C	302

[a] Referred to the PBI polymer.
[b] Referred to the PBI polymer.
[c] Phosphoric acid solution uptake estimated according to Eq. (1).

membranes in comparison with 30% porous PBI membrane data set (202 wt.% vs. 420 wt.%). SEM analyses could provide us with valuable information to explain the attained results. Micrographs of porous hybrid PBI membrane compared to pure counterpart (45% porosity) are shown in Fig. 18 to illustrate the homogeneous distribution of the inorganic particles along and across the membrane thickness (around 60 μm) before phosphoric acid doping. The most remarkable feature is the sponge-like porous structure 45% in porosity obtained after DBP leaching with interconnected pores of 2–4 μm in diameter and a dense skin layer formed on the glass plate side around 5 μm in thickness. In general, the porogen method allows control over the porosity level (the higher porogen content the higher pore size and total pore volume) and the morphology by adjusting the porogen/PBI ratio and the chemical nature of the porogen [27]. In this work, the addition of DBP porogen in a 45 wt.% referred to the polymer, provides on one hand with interconnected pores, well-suited to attain uninterrupted proton conduction pathways after phosphoric acid doping. But, on the other hand, durability issues related to the phosphoric acid leakage are likely to occur. In contrast, for 30% porosity level, isolated spherical pores, most adequate for conductor confinement, are preferably formed.

Alike dense systems, the phosphoric acid uptake values are higher for porous hybrid PBI/SO_3H-ETS-10 membranes. In addition, their conduction properties correlate quite well with the concentration of proton conductors attained (i.e. always above the pure porous PBI values). This behaviour is quite distinct from dense membranes and is a consequence of the different proton conduction pathways available at the surface: (i) acid-PBI sites; (ii) SO_3H-ETS-10-PBI sites; and, (iii) free phosphoric acid an water molecules. At 150 °C, the porous hybrid membranes exhibit 80 mS cm^{-1} and 75 mS cm^{-1} when doped at 50 °C and 25 °C, respectively; in comparison with 60 mS cm^{-1} and 48 mS cm^{-1} for pure counterparts.

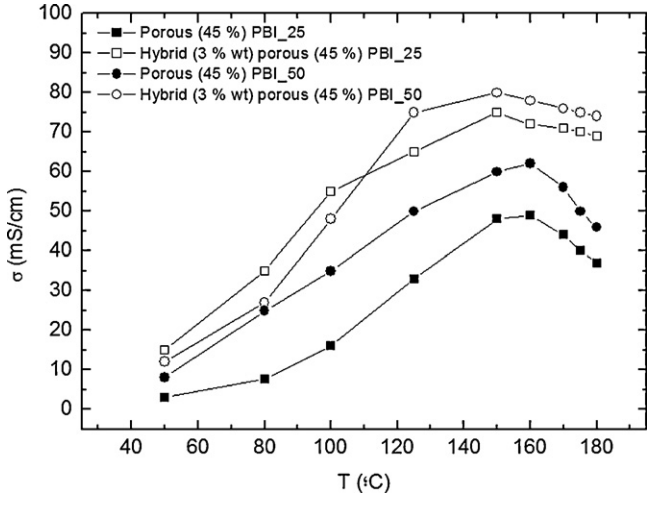

Fig. 17. "In-plane" conductivity measurements of porous systems (45% in porosity) after phosphoric acid doping at 25 °C and 50 °C: pure PBI membrane vs. hybrid PBI membrane with 3 wt.% of SO_3H-ETS-10.

Moreover, the benefits imposed by the inclusion of SO_3H-ETS-10 crystals to the porous PBI membrane (45% in porosity) are also remarkable in the high temperature region (above 150 °C) where phosphoric acid oligomerization usually leads to the formation of pyrophosphoric acid ($H_4P_2O_7$) and the conductivity drops [18,19]. As it can be observed in Fig. 17, this effect is quite less notorious for hybrid samples. As an example, at 180 °C, the porous hybrid membranes exhibit 74 mS cm^{-1} and 69 mS cm^{-1} when doped at 50 °C and 25 °C, respectively; in comparison with 46 mS cm^{-1} and 36 mS cm^{-1} for pure counterparts. This behaviour could be explained by the most effective acid-doping of PBI polymer due to the "positive" sulfonic–phosphoric acid interactions already pointed out.

Considering that the PBI based membranes doped at 50 °C outperformed those prepared at 25 °C, further analyses were carried out on these samples. Table 3 shows water and phosphoric acid loadings determined by TGA to provide with a more realistic values. For both conducting species, two main desorption/decomposition peaks have been identified by means of the differential analyses (see Fig. 19a). In the case of water molecules, the desorption of weakly bonded molecules takes place at temperatures below 100 °C. On the other hand, strongly bonded molecules are released at temperatures around 150–170 °C; but always higher for dense samples due to diffusional desorption limitations. Considering the water uptake capability of SO_3H-ETS-10 (see Fig. 9) and the relative low inorganic loading of the hybrid membranes; it can be concluded that the water management behaviour observed for dense membranes is mainly due to the hydrophilic PBI matrix. On the contrary, it is quite noteworthy the behaviour shown by porous membranes. The higher surface area imposed by the 45% porosity level in the macropore range (2–4 μm) leads to a markedly enhancement of physisorbed water contribution (above 21 wt.%); which indeed is drastically reduced when a 3% of SO_3H-ETS-10 loading is present (below 2 wt.%). Therefore, better mechanical properties and prolonged life time would be expected for such porous hybrid membranes. Again, this experimental observation is underlying the blocking of pristine PBI reactivity by sulfonic-ETS-10 crystals.

Whatever the case, the proton conduction performance above 150 °C is mainly related to the phosphoric acid loading. For this intrinsic conductor, two main peaks at 190–210 °C and 490–600 °C corresponding to the 1st and 2nd dehydration of phosphoric acid molecules are clearly distinguished (see Fig. 19a). In general, the H_3PO_4 thermal events are broaden and shifted to lower temper-

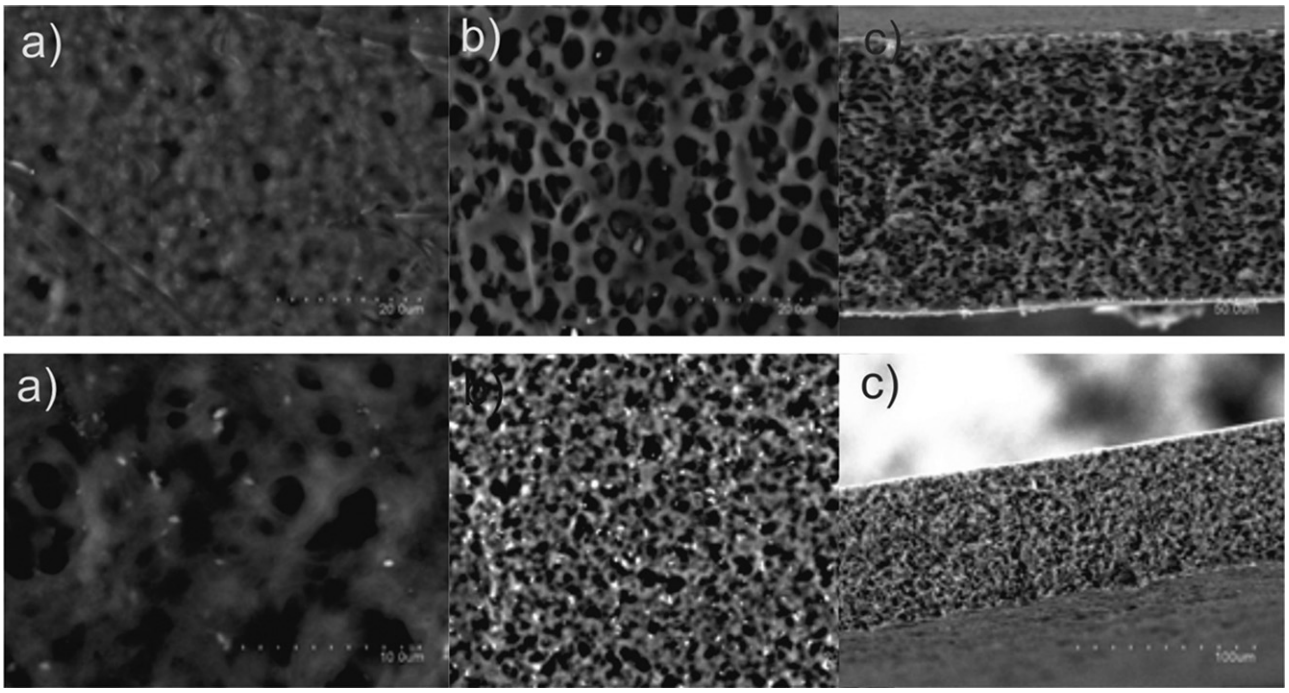

Fig. 18. SEM analyses of porous PBI systems (45% in porosity) before phosphoric acid doping: (a) bottom (glass side) surface, (b) top (air side) surface and (c) cross section. Upper part: pure PBI membrane; lower part: hybrid PBI membrane with 3 wt.% of SO_3H-ETS-10.

atures for porous membranes due to higher amounts of free acid molecules are being decomposed at improved desorption rates. For dense membranes, the H_3PO_4 loading estimated for pristine PBI is the highest (10.5% vs. 9.0%) unlike acid uptake values estimated by Eq. (1). For 45% porous membranes, the H_3PO_4 loading estimated for pristine PBI is the lowest (13.4% vs. 18.6%) in accordance with values reported in Table 2. Once again, this experimental observation is underlying the "positive" sulfonic-phosphoric acid interactions on the doping stage and conduction properties. In addition, a deficient filling of the total pore volume by phosphoric acid molecules is encountered when the experimental H_3PO_4 loadings are compared to theoretical values assuming a total coverage of the original membrane porosity (around 15–30% of the total pore volume). It is well-known that PBI membranes exhibit a volume swelling after phosphoric acid impregnation resulting in separation of the polymer backbones [8,37]. Nevertheless, in our case, for macroporous membranes, this effect leads to a reduction in the pore size and porosity level. Thus, SEM and Hg-porosimetry analyses of doped porous PBI membranes are under investigation for a better understanding. Above all, it is clear that the porous PBI structure (pore size, connectivity and asymmetry) has to be carefully tailored to ensure an adequate amount of embedded proton conductor and to avoid its leakage during handling.

The H_3PO_4/H_2O wt. ratio has also been included in Table 3 in an attempt to explain the conduction behaviour not only in the whole temperature range; but also at temperatures above 150 °C where phosphoric oligomerization takes place. Accounting from the tabulated values, it is clearly outstanding the porous SO_3H-ETS-10/PBI membrane (2.38) followed by dense PBI (0.87), dense SO_3H-ETS-10/PBI (0.79) and porous PBI (0.5). This sequence is in agreement with the conductivity plateau exhibited by porous SO_3H-ETS-10/PBI membrane (see Fig. 17) and also with the proton conduction properties of the whole set.

Finally, at temperatures above 600 °C the thermal events corresponding to PBI decomposition have been recorded. For hybrid membranes the differential analyses at temperatures above 700 °C (see Fig. 19b), allows the identification of a new decomposition peak at 830 °C associated to PBI moieties strongly linked to the inorganic crystals by means of sulfonic–amino interactions.

The methanol permeability values registered with the experimental set-up shown in Fig. 5 at room conditions, 50 °C, 100 °C and 150 °C are depicted in Fig. 20 in comparison with Nafion 117 and dense PBI data extracted from literature [38]. It is noteworthy that the methanol permeability of the doped membranes herein prepared is of about one-tenth/one hundredth, for porous or dense systems, respectively, of the value read with Nafion 117. Moreover, the methanol cross-over estimated at 180 °C by real time electrochemical mass spectrometry for PBI by Savinell et al. [38], is on the same order of magnitude (1.5×10^{-10} mol (cm s bar)$^{-1}$) that those evaluated in this work by vapour permeation measurements (1.2×10^{-10} mol (cm s bar)$^{-1}$). Unlike it was expected, all the doped membranes tested (porous and dense) exhibited the same methanol permeability pattern decreasing with temperature. However, before phosphoric acid doping the permeation through porous membranes (not shown here) is quite distinct. As a matter

Table 3
Water and phosphoric acid loadings estimated by TGA analyses for some of the PBI based membranes prepared.

Sample	% H_2O (1)	% H_2O (2)	% H_2O (total)	% H_3PO_4 (1)	% H_3PO_4 (2)	% H_3PO_4 (total)	H_3PO_4/H_2O (wt. ratio)
Dense PBI	6.7	5.4	12.1	7.6	2.9	10.5	0.87
Hybrid (3 wt.%) dense PBI	7.1	4.3	11.4	5.3	3.7	9.0	0.79
Porous (45%) PBI	21.3	5.3	26.6	5.9	7.5	13.4	0.50
Hybrid (3 wt.%) porous (45%) PBI	1.7	6.1	7.8	4.7	13.9	18.6	2.38

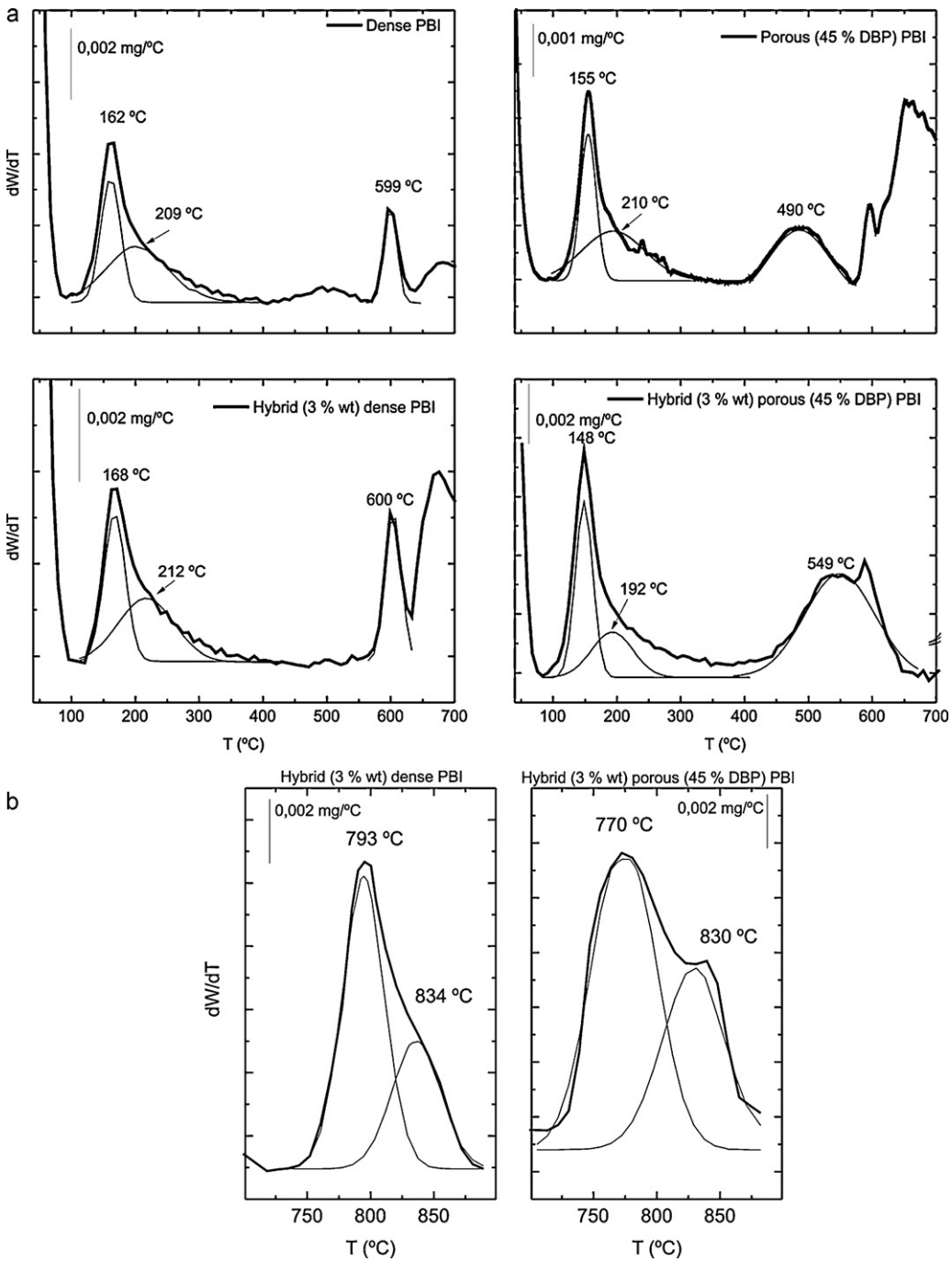

Fig. 19. Thermogravimetric differential curves of dense and porous systems after phosphoric acid doping at 50 °C for: (a) phosphoric acid evaluation up to 700 °C and (b) PBI decomposition.

of fact, permeability increases with temperature in the full operation range in agreement with the prevailing gas phase diffusion mechanism through the membrane pores. Moreover, for a given temperature, the permeability is always higher for undoped porous membranes, supporting the hypothesis of the porosity collapse by swelling [37] during doping stage and/or plasticization [39] under methanol permeation conditions. In spite of PBI itself has very strong hydrogen bonding which may help to suppress swelling, a porous PBI structure with stronger polarity is prone to physico-chemical interactions with permeating polar methanol molecules. To get insight this effect, additional post-mortem characterization tests are in progress.

Accounting from Eq. (3) the observed behaviour is easily explained by a decrease of the methanol solubility factor ($1/H$). In general, permeability values for hybrid membranes are higher than pure counterparts, although the differences are not quite noticeable in agreement with the good compatibility SO_3H-ETS-10/PBI already discussed (i.e. 2.4×10^{-10} vs. 1.2×10^{-10} mol (cm s bar)$^{-1}$, and 1.1×10^{-9} vs. 1.0×10^{-9} mol (cm s bar)$^{-1}$; for dense and porous systems, respectively). However, at 150 °C the behaviour is just the opposite; hybrid PBI counterparts outperform pure PBI membranes. This fact would be in agreement with a more prevailing role of ETS-10 micropores for activated methanol diffusion at higher temperatures. Nevertheless, the porous structure of PBI

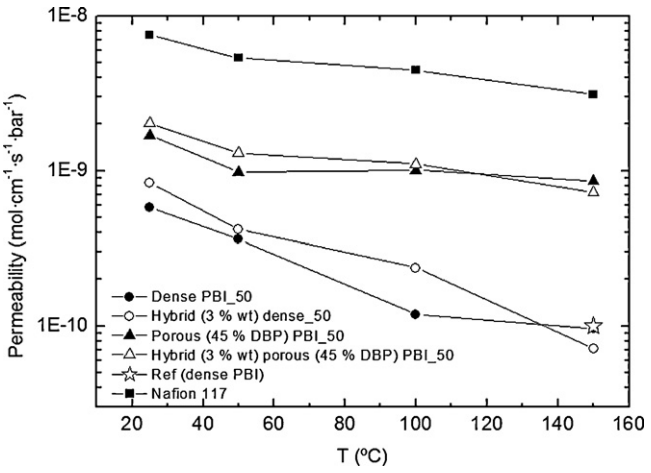

Fig. 20. Methanol permeability measurements in vapour phase for dense and porous systems after phosphoric acid doping at 50 °C. Reference value adapted from [38].

Table 4
Membrane selectivity values expressed as conductivity/methanol permeability ratio as a function of temperature for some of the PBI based membranes prepared.

Sample	Conductivity/permeability ratio (S·s·bar mol^{-1})		
	T = 50 °C	T = 100 °C	T = 150 °C
Dense PBI	4.7E+6	1.3E+8	2.3E+8
Hybrid (3 wt.%) dense PBI	2.5E+6	2.6E+7	2.5E+8
Porous (45% DBP) PBI	6.2E+5	4.9E+6	8.9E+6
Hybrid (3 wt.%) porous (45% DBP) PBI	3.4E+6	1.9E+7	4.9E+7
Nafion 117	1.4E+6	3.8E+5	6.3E+4

membranes required further optimization to reduce methanol cross-over.

To summarize, the transport selectivity of the as prepared dense and porous membranes has been evaluated by comparison of the conductivity/methanol permeability values at 50 °C, 100 °C and 150 °C (see Table 4). As a result, dense pure PBI membrane is preferred at 50 °C (4.7×10^6 S·s·bar mol^{-1}); whereas at 150 °C, dense PBI + 3% SO_3H-ETS-10 membranes exhibit the higher conductivity/methanol permeability ratio (2.5×10^8 S·s·bar mol^{-1}).

4. Conclusions

Novel hybrid membranes based on polybenzimidazole (PBI) and ETS-10 titanosilicate type material functionalized with sulfonic groups have been successfully developed for high temperature proton exchange membrane fuel cells (HT PEMFCs) applications.

Firstly, the organic functionalization of the external surface of microporous ETS-10 crystals in a 4 wt.%, has allowed to improve the intrinsic conductivity of the inorganic loading attaining proton conductivity values as high as 30 mS cm^{-1} at 150 °C under saturated conditions. This fact is due to the coexistence of the two main conduction mechanisms: vehicle-type mechanism (with H_2O as proton carrier) and hopping-type mechanism (through –SO_3H terminal groups + H_2O molecules).

Secondly, a parametric study on the inorganic loading effect onto conduction performance of dense membranes has been carried out to identify an optimum value around 3 wt.% referred to the polymer in the studied range (1–20 wt.%). This fact is due to the sulfonic acid groups grafted onto ETS-10 crystals contribute to a most effective acid-doping of PBI polymer and provide new proton conduction pathways. A synergic combination of both effects occurs for dense PBI/SO3H-ETS-10 with a 3 wt.% of inorganic loading which reveals as the most adequate among the tested (i.e. 55 mS cm^{-1} at 170 °C as "in-plane" conductivity).

With the aim to promote even more the conductivity of hybrid membranes, porous based PBI membranes have also been prepared by using DBP as porogen-template. A quite distinct porous structure is ascertained from phosphoric acid uptake values, conduction performance and SEM observations of both 30% and 45% porous data set. The addition of DBP porogen in a 30 wt.% renders in isolated spherical pores, most adequate for conductor confinement but with poorer cross-conductivity potentialities. As a result, the porous hybrid PBI membrane with a 3% of SO_3H-ETS-10 emerges as the most adequate among the tested (i.e. 50 mS cm^{-1} at 160 °C as surface conductivity) because the conduction performance is almost similar to pure porous PBI but at a clearly lower H_3PO_4 doping levels (185% vs. 420%), and as a consequence improved durability properties will be expected.

On the contrary, for 45% porosity level, interconnected pores, well-suited to attain uninterrupted proton conduction pathways after phosphoric acid doping are preferably formed; but, on the other hand, durability issues related to the phosphoric acid leakage are likely to occur. The higher surface area imposed by the 45% porosity level and macropore size (2–4 μm) leads to a markedly enhancement of physisorbed water contribution (above 21 wt.%); which indeed is drastically reduced when a 3% of SO_3H-ETS-10 loading is present due to the blocking of pristine PBI reactivity by sulfonic-ETS-10 crystals. Accordingly, better mechanical properties and prolonged life time would be expected for such porous hybrid membranes. The H_3PO_4 loading estimated by TGA for pristine porous PBI is the lowest (13.4% vs. 18.6% after doping at 50 °C) underlying the "positive" sulfonic-phosphoric acid interactions on the doping stage and conduction properties. In particular, at 150 °C, the porous hybrid membranes exhibit 80 mS cm^{-1} and 75 mS cm^{-1} when doped at 50 °C and 25 °C, respectively; in comparison with 60 mS cm^{-1} and 48 mS cm^{-1} for pure counterparts. Moreover, these benefits on "in-plane" conduction performance are also remarkable above 140 °C due to a conductivity plateau is observed in the typical region where pyrophosphoric acid is formed. Thus, at 180 °C, the porous hybrid membranes exhibit 74 mS cm^{-1} in comparison with 46 mS cm^{-1} for pure counterparts after doping at 50 °C in agreement with the estimated H_3PO_4/H_2O wt. ratio by TGA.

The methanol permeability of the as prepared PBI based membranes is of about one-tenth (for porous membranes)/one hundredth (for dense membranes), of the value read with Nafion 117 and of the same order of magnitude (1.5×10^{-10} mol (cm s bar)$^{-1}$ at 150 °C for pure dense PBI) than those reported in the literature by electrochemical mass spectrometry. The depicted methanol permeability pattern with temperature for all the prepared doped PBI based membranes is easily explained by a decrease in methanol solubility ($1/H$). This observation is indicating that no non-selective defects are formed at the organic-inorganic interface and pronounced membrane swelling takes place in porous systems. In general, permeability values for hybrid membranes are slightly higher than pure counterparts at temperatures up to 100 °C. However, at 150 °C the behaviour is just the opposite in accordance with a more prevailing role of ETS-10 micropores for activated methanol diffusion.

The transport selectivity of the as prepared dense and porous membranes has been evaluated by comparison of the "in-plane" conductivity/methanol permeability values. As a result dense PBI and dense PBI + 3% SO_3H-ETS-10 membranes reveal as the most adequate at 50 °C and 150 °C, respectively. In addition, preliminary fuel cell testing with H_2/methanol fuels and O_2/air oxidants are being performed.

As a general conclusion, the porous structure of PBI membranes requires further optimization to exploit their proton conduction potentialities. New porogen-type molecules (i.e. triphenyl phosphate), and porosity values (from 30 wt.% to 80 wt.%) are being discussed for a future publication.

Acknowledgement

The authors would like to acknowledge financial support from the European Commission through the FP7 funded project ZEOCELL (http://ina.unizar.es/zeocell): Grant Agreement no: 209481.

References

[1] Multi-Annual Implementation Plan 2008-2013. (http://www.fch-ju.eu/page/documents).
[2] Energy 2020: A strategy for competitive, sustainable and secure energy. (http://eur-lex.europa.eu/LexUriServ/LexUriServ.do?uri=COM:2010:0639:FIN:EN:HTML).
[3] Q. Li, J.O. Jensen, R.F. Savinell, N.J. Bjerrum, Prog. Polym. Sci. 34 (2009) 449–547.
[4] J.A. Asensio, E.M. Sanchez, P. Gomez-Romero, Chem. Soc. Rev. 39 (8) (2010) 3210–3239.
[5] Savinell, R.F., Litt, M.H. Proton conducting polymers used as membranes. 5,525,436, U.S. Patent, 1996.
[6] J.T. Wang, R.F. Savinell, J. Wainright, M. Litt, H. Yu, Electrochim. Acta 41 (1996) 193–197.
[7] J. Lobato, P. Cañizares, M.A. Rodrigo, J.J. Linares, G. Manjavacas, J. Membr. Sci. 280 (2006) 351–362.
[8] J. Lobato, P. Cañizares, M.A. Rodrigo, J.J. Linares, J.A. Aguilar, J. Membr. Sci. 306 (2007) 47–55.
[9] R.H. He, Q.F. Li, A. Bach, J.O. Jensen, N.J. Bjerrum, J. Membr. Sci. 277 (2006) 38–45.
[10] Q. Li, J.O. Jensen, C. Pan, V. Bandur, M. Nilsson, Schönberger, Fuel Cells 8 (2008) 188–199.
[11] Q. Li, C. Pan, J.O. Jensen, P. Noyé, N.J. Bjerrum, Mater. Chem. 19 (2007) 350–352.
[12] R.H. He, Q.F. Li, G. Xiao, N.J. Bjerrum., J. Membr. Sci. 226 (2003) 169–184.
[13] P. Staiti, M. Minutoli, S. Hocevar, J. Power Sources 90 (2000) 231–235.
[14] P. Staiti, M. Minutoli, J. Power Sources 94 (2001) 9–13.
[15] Q. Li, Z.G. Shao, K. Scott, J. Power Sources 183 (2008) 69–75.
[16] S.Y.-L. Liu, J. Membr. Sci. 332 (2009) 121–128.
[17] J.A. Mader, B.C. Benicewicz, Macromolecules 43 (2010) 6706–6715.
[18] K. Scott, S. Pilditch, M.J. Mamlouk, Appl. Electrochem. 37 (2007) 1245–1259.
[19] T. Sancho, J. Lemus, M. Urbiztondo, J. Soler, M.P. Pina, Micropor. Mesopor. Mater. 115 (1) (2008) 206–213.
[20] X. Li, E.P.L. Roberts, S.M. Holmes, V. Zholobenko, Solid State Ionics 178 (2007) 1248–1255.
[21] M. Sadeghi, M.A. Semsarzadeh, H. Moadel, J. Membr. Sci. 331 (2009) 21–30.
[22] S. Choi, J. Coronas, Z. Lai, D. Yust, F. Onorato, M. Tsapatsis, J. Membr. Sci. 316 (2008) 145–152.
[23] S.-W. Chuang, S.C-L. Hsu, C.-L. Hsu, J. Power Sources 168 (2007) 172–177.
[24] T.-C. Wei, H.W. Hillhouse, J. Phys. Chem. B 110 (2006) 13728–13733.
[25] T. Sancho, J. Soler, M.P. Pina, J. Power Sources 169 (2007) 92–97.
[26] J. Rocha, A. Ferreira, Z. Lin, M.W. Anderson, Micropor. Mesopor. Mater. 23 (1998) 253–263.
[27] D. Mecerreyes, H. Grande, O. Miguel, E. Ochoteco, R. Marcilla, I. Cantero, Chem. Mater. 16 (2004) 604–607.
[28] Blázquez, A., Miguel, O., Garrido, O., van de Ven, E., Borneman, Z., Soler, J., Pina, M.P. A nanostructured electrolyte porous membrane based on polymers and functionalized microporous nanocrystals for FCs applications. PCT application number: PCT/EP2010/064857.
[29] F. Alcaide, G. Álvarez, L. Ganborena, J. Iruin, O. Miguel, J.A. Blazquez, Polym. Bull. 62 (2009) 813–827.
[30] M.B. Rao, S. Sircar, J. Membr. Sci. 85 (1993) 253–264.
[31] Y. Wang, D. Yang, X. Zheng, Z. Jiang, J. Li, J. Power Sources 183 (2008) 454–463.
[32] K.A. Mauritz, R.B. Moore, Chem. Rev. 104 (2004) 4535–4586.
[33] T. Chou, Biophys. J. 86 (2004) 2827–2836.
[34] S. Woutersen, H. Bakker, Phys. Rev. Lett. 96 (2006) 138305.
[35] K.D. Kreuer, Chem. Mater. 8 (1996) 610–641.
[36] S.W. Chuang, S.L.C. Hsu, Y.H. Liu, J. Membr. Sci. 305 (2007) 353–363.
[37] S.C. Kumbharkar, M.N. Islam, R.A. Potrekar, U.K. Kharul, Polymer 50 (6) (2009) 1403–1413.
[38] J.T. Wang, S. Wasmus, R.F. Savinell, J. Electrochem. Soc. 143 (4) (1996) 1233–1239.
[39] G. Kung, L.Y. Jiang, Y. Wang, T.-S. Chung, J. Membr. Sci. 360 (2010) 303–314.